

HySCO

Hyperelastic Susceptibility Artifact Correction of DTI in SPM

Lars Ruthotto¹, Siawoosh Mohammadi², Constantin Heck¹, Jan Modersitzki¹,
Nikolaus Weiskopf²

¹Institute of Mathematics and Image Computing, Universität zu Lübeck

²Wellcome Trust Center for Neuroimaging, University College London

`lars.ruthotto@mic.uni-luebeck.de`

Abstract. Echo Planar Imaging (EPI) is a MRI acquisition technique that is the backbone of widely used investigation techniques in neuroscience like, e.g., Diffusion Tensor Imaging (DTI). While EPI offers considerable reduction of the acquisition time one major drawback is its high sensitivity to susceptibility artifacts. Susceptibility differences between soft tissue, bone and air cause geometrical distortions and intensity modulations of the EPI data. These susceptibility artifacts severely complicate the fusion of micro-structural information acquired with EPI and conventionally acquired structural information.

In this paper we introduce a new tool for hyperelastic susceptibility correction of DTI data termed **HySCO** that is integrated into the Statistical Parametric Mapping (SPM) software as a toolbox. Our new correction pipeline is based on two datasets acquired with reversed phase encoding gradients. For the correction, we integrated the variational image registration approach by Ruthotto et al. [1] into the SPM batch mode. We briefly review the model, discuss involved parameter settings and exemplarily demonstrate **HySCO**'s effectiveness on a human brain DTI dataset.

1 Introduction

Echo Planar Imaging (EPI) is a commonly available ultrafast MRI acquisition technique [2]. It is routinely used for key investigation techniques in modern neuroscience like, e.g., Diffusion Tensor Imaging (DTI) [3] or functional MRI.

While offering a considerable reduction of acquisition time, a drawback of EPI is the low bandwidth in phase-encoding direction. Therefore, EPI is highly sensitive to inhomogeneities in the magnetic field. In practice, the MRI scanner's almost perfectly homogeneous magnetic field is perturbed by the different magnetic susceptibilities of soft tissue, bone and air associated with the subject. Field inhomogeneities cause geometrical distortions and intensity modulations, the so-called *susceptibility artifacts* in EPI. Susceptibility artifacts considerably complicate the fusion of functional and micro-structural information acquired using EPI with conventionally acquired anatomical image data, for which susceptibility artifacts are almost negligible [1].

A number of approaches have been proposed to reduce susceptibility artifacts in EPI. For instance, *fieldmap* methods measure the inhomogeneities by a reference scan and subsequently correct the data [4]. An alternative is the *reversed gradient method* presented by [5]. It requires the acquisition of an image pair, acquired using phase encoding gradients of positive and negative polarity, which results in oppositely distorted data. Subsequently, the data are corrected for susceptibility artifacts using modified image registration approaches like, e.g., [5,6,7,1].

In this work, we present a novel hyperelastic susceptibility correction pipeline termed **HySCO**, which is integrated as a batch tool into the *Statistical Parametric Mapping* (SPM) toolbox (<http://www.fil.ion.ucl.ac.uk/spm/>). The backbone of HySCO is a reversed gradient method and the freely available toolbox FAIR [8] that features also the code underlying [1]. The key feature of the scheme [1] is a tailored regularization functional inspired by hyperelasticity that ensures invertibility of the geometric transformations. We integrated the new pipeline into SPM to allow convenient susceptibility artifact correction of large datasets. We exemplify the effectiveness of the method on a human brain DTI dataset. HySCO will be made freely available after publication.

2 Materials and Methods

2.1 Data Acquisition

One healthy, male volunteer was scanned on a TIM Trio 3T scanner (Siemens Healthcare, Erlangen, Germany) with written informed consent. The acquisition protocol provides two DTI datasets: 66 images with positive phase encoding \mathcal{I}_1^k and 66 images with negative phase encoding \mathcal{I}_2^k , where $k = 1, \dots, 66$. Each DTI dataset was acquired using the following parameters: 6 non-diffusion-weighted (DW) images (image number: $k = 1, \dots, 6$), 60 DW images with spherically distributed diffusion-gradient directions (image number: $k = 7, \dots, 66$), matrix 96×96 , 60 slices, 2.3mm isotropic resolution, 5/8 Partial Fourier in PE direction using zero filling reconstruction, TE=86ms, volume TR=10.5ms. Note that for each pair of images, \mathcal{I}_1^k and \mathcal{I}_2^k , the diffusion direction and diffusion-weighting was the same in both datasets. We thus assumed that differences in \mathcal{I}_1^k and \mathcal{I}_2^k were mostly due to field inhomogeneities.

2.2 Hyperelastic Susceptibility Correction of Echo-Planar MRI

We briefly summarize the numerical implementation of the reversed gradient method in [1]. Given are two oppositely distorted images \mathcal{I}_1 and \mathcal{I}_2 . Based on the physical distortion model derived in [5], the goal is to estimate the field inhomogeneity $B : \Omega \rightarrow \mathbb{R}$ by minimizing the distance functional

$$\mathcal{D}[B] = \frac{1}{2} \int_{\Omega} (\mathcal{I}_1(x + B(x)v) (1 + \partial_v B(x)) - \mathcal{I}_2(x - B(x)v) (1 - \partial_v B(x)))^2 dx, \quad (1)$$

where v denotes the phase-encoding direction, typically $v = (0, 1, 0)^T \in \mathbb{R}^3$ is the second unit vector. The transformations applied to the images have two components: A displacement that is restricted along v and an intensity modulation given by the Jacobian determinant of the geometrical transformation [5]. Note the opposite signs of the displacement and intensity modulations for \mathcal{I}_1 and \mathcal{I}_2 . Following [1], the field inhomogeneity is estimated numerically by solving

$$\min_B \mathcal{J}[B] := \mathcal{D}[B] + \alpha \mathcal{S}^{\text{diff}}[B] + \beta \mathcal{S}^{\text{jac}}[B], \quad (2)$$

where $\mathcal{S}^{\text{diff}}$ is a diffusion-, and \mathcal{S}^{jac} is a nonlinear regularization term that ensures $-1 < \partial_v B < 1$, which translates to invertible geometrical transformations and positive intensity modulations. The parameters $\alpha, \beta > 0$ balance between minimization of the distance and the regularization functionals.

Problem (2) is solved using the publicly available registration framework FAIR [8] in Matlab. More precisely, a regularized cubic B-spline interpolation is used as image model, where a regularization parameter $\theta \geq 0$ can be used to improve robustness against noise; see [8] for details. Problem (2) is discretized on a coarse to fine hierarchy of discretization levels and solved on each level using a Gauss Newton optimization scheme. The coarse grid solution is used as a starting guess for the optimization on the fine grid; see [8] for details.

2.3 Susceptibility Artifact Correction Pipeline for DTI in the SPM Batch Mode

Before tensor estimation two pre-processing steps were applied. First, the non-DW and DW images were corrected for motion and eddy current effects using the ECMOCO toolbox; see [9] for details on preprocessing. Second, each image was corrected for susceptibility artifacts using three different methods: (a) none, (b) the fieldmap toolbox ([4] following the pipeline described in [9]), and (c) the HySCO toolbox. The diffusion tensors and the root-mean square of the tensor-fit error ($\text{rms}(\epsilon)$) were estimated for the DTI datasets \mathcal{I}_1 and \mathcal{I}_2 using ordinary least squares as in [9].

In the first step of the HySCO method we solved Problem (2) for the non-diffusion weighted images \mathcal{I}_1^1 and \mathcal{I}_2^1 ; see Fig. 1. To this end, we used the above outlined multilevel strategy with three discretization levels $24 \times 24 \times 15$, $48 \times 48 \times 30$, and $96 \times 96 \times 60$. Thereby, we obtained an estimate of the field inhomogeneity denoted by B^1 . Subsequently, we solved (2) for \mathcal{I}_1^k and \mathcal{I}_2^k on the finest discretization level with the starting guess B^1 and obtained B^k for $k = 2, \dots, 66$. These correction steps account for small variations in the field inhomogeneity arising from other effects like residual eddy currents [10]. Finally, the corrected images are obtained by applying the transformations in (1) for B^k on \mathcal{I}_1^k and \mathcal{I}_2^k .

For convenient access to the correction scheme, we designed a graphical user interface in the batch mode of SPM. The user can control the regularization parameters (default: $\alpha = 50, \beta = 10$), the resolutions of the levels in the multilevel strategy, and the smoothing parameter (default: $\theta = 0.01$).

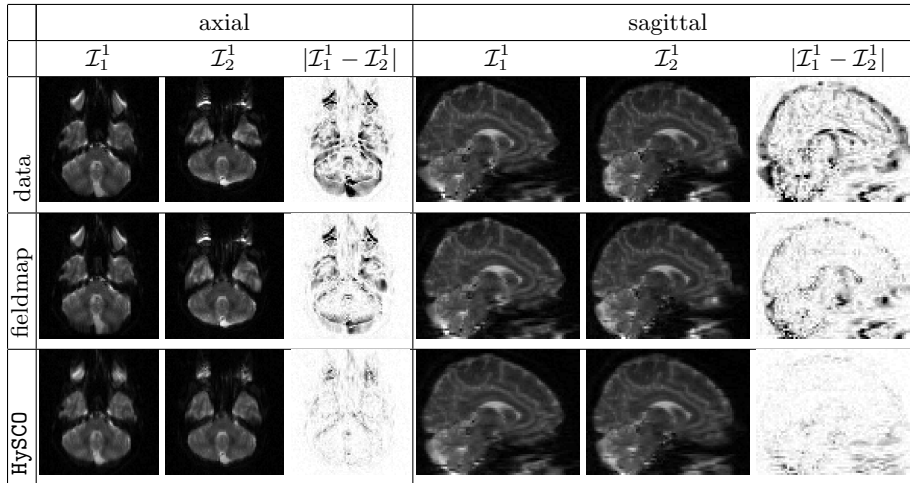


Fig. 1. Effect of 3D susceptibility artifact correction. We visualize axial (left) and sagittal (right) projections of the images \mathcal{I}_1^1 and \mathcal{I}_2^1 , acquired without diffusion weighting. The oppositely distorted images and their absolute difference are depicted using equally scaled intensities. Considerable susceptibility artifacts manifest in the original data; compare image pairs in first row. Using the SPM fieldmap toolbox improved the similarity of \mathcal{I}_1^1 and \mathcal{I}_2^1 , however, structures in the difference image remained; see second row. Superior correction results were obtained using the proposed HySCO method; see third row.

2.4 Comparison of Susceptibility Artifact Correction Methods

We compared the correction results of the fieldmap correction and HySCO based on two criteria. As a first step, we compared the similarity of the first image pair acquired without diffusion weighting, i.e., $k = 1$. To this end, we used visual assessment of uncorrected, fieldmap corrected, and HySCO corrected image pairs, as well as their respective difference images given by (1). In a second step, we compared the impact of the correction pipeline on the diffusion tensor reconstruction using visual inspection of the $\text{rms}(\epsilon)$ maps as well as quantification of the $\text{rms}(\epsilon)$ over the whole brain.

3 Results

In Fig. 1 we visualize axial and sagittal slices of the original 3D data, fieldmap corrected data, and results of HySCO. Severe distortions manifest in the original data, especially at the transition between bone and air; compare images in first row and difference images. Similarity between both images was increased by the fieldmap correction indicated by a reduction of the distance functional in (2) from 100% to 52.91%; see second row in Fig. 1. A considerable improvement was achieved by HySCO, which relies on the correction scheme [1]. The image pairs

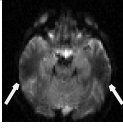
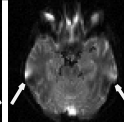
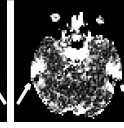
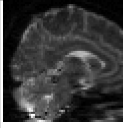
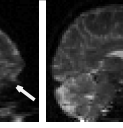
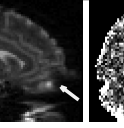
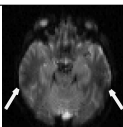
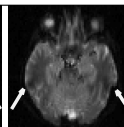
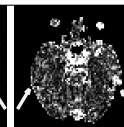
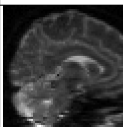
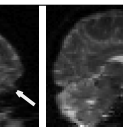
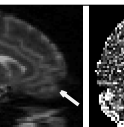
	axial			sagittal		
	\mathcal{I}_1^1	\mathcal{I}_2^1	rms(ϵ)	\mathcal{I}_1^1	\mathcal{I}_2^1	rms(ϵ)
fieldmap						
HySCO						

Fig. 2. Impact of susceptibility correction methods on tensor-fit error rms(ϵ) (axial and sagittal slices). The root-mean square of rms(ϵ) (3rd and 6th column) and the non-diffusion weighted images \mathcal{I}_1^1 and \mathcal{I}_2^1 (1st, 2nd, 4th, and 5th column) are visualized. The tensor-fit error is larger in regions, where the effect of susceptibility artifacts has been insufficiently corrected; see, e.g., bright spots at the sinuses and frontal areas, highlighted by arrows. Over the whole brain HySCO yielded a considerably smaller average tensor-fit error as compared to the fieldmap correction; 0.1 mm²/s vs. 0.15 mm²/s.

were visually almost indistinguishable; see third row in Fig. 1. The superiority manifests also in the reduction of the distance functional to 8.8%. The multi-level correction required about 20 seconds on a current standard computer.

The distance between the image pairs \mathcal{I}_1^k and \mathcal{I}_2^k , where $k = 2, \dots, 66$, was on average reduced from 100% to 50% for the fieldmap correction. By applying the transformation model described in (1) with the inhomogeneity estimate B^1 from the first problem the image distance was on average reduced to 38.4%. Best results were obtained by performing correction steps on the finest resolution with an average distance reduction to 18.1%. All intensity modulations were positive and overall in a range between 0.03 and 1.97. The average runtime for the correction steps was around 12 seconds on a current standard computer.

Fig. 2 shows axial and sagittal slices of the fieldmap and HySCO corrected non-diffusion-weighted images and tensor-fit error maps. Using the HySCO method resulted in a smaller tensor-fit error than when using the fieldmap method; see, e.g., bright spots in the sinuses and frontal areas highlighted by arrows. The mean tensor fit error over the whole brain was 0.15 mm²/s for the fieldmap approach and 0.1 mm²/s for HySCO.

4 Discussion

We introduced HySCO, a novel pipeline for susceptibility artifact correction of DTI data. Our pipeline requires two DTI datasets, acquired with reversed phase encoding gradients and thus opposite distortion effects. The backbone of our pipeline is the susceptibility correction scheme presented in [1]. HySCO is integrated as a toolbox into the Statistical Parametric Mapping (SPM) software

in Matlab. To enable convenient processing of large datasets, a graphical user interface was designed and integrated into the batch mode of SPM.

In our pipeline, the first image pair, acquired without diffusion weighting, is corrected for susceptibility artifacts using a multi-level strategy. Based on this starting guess correction steps are performed for the diffusion weighted images. This leads to a considerable reduction of computation times, which is desirable for the correction of DTI datasets with many diffusion measurements.

The proposed pipeline requires the acquisition of two DTI datasets and thus doubles scan time, which might not always be feasible. As our results indicate, however, even solving the correction problem once for non-diffusion weighted images and applying the transformation to the remaining image volumes can considerably reduce susceptibility artifacts. In this case, only one image needs to be acquired with reversed phase encoding gradients. This case is also covered by our HySCO implementation.

Preliminary results indicate that HySCO gives superior correction results compared to fieldmap approaches, e.g., [4], with respect to image similarity and tensor fit error. Extensive evaluations will be a main focus of future work. Further, combinations with other correction techniques like, e.g., [9] will be investigated.

References

1. Ruthotto L, Kugel H, Olesch J, Fischer B, Modersitzki J, Burger M, et al. Diffeomorphic Susceptibility Artefact Correction of Diffusion-Weighted Magnetic Resonance Images. *Physics in Medicine and Biology*. 2012;57:5715–5731.
2. Stehling M, Turner R, Mansfield P. Echo-planar imaging: magnetic resonance imaging in a fraction of a second. *Science*. 1991;254(5028):43–50.
3. Le Bihan D, Mangin J, Poupon C. Diffusion tensor imaging: concepts and applications. *Journal of Magnetic Resonance Imaging*. 2001;13:534–546.
4. Hutton C, Bork A, Josephs O, Deichmann R, Ashburner J, Turner R. Image Distortion Correction in fMRI: A Quantitative Evaluation. *NeuroImage*. 2002;16(1):217–240.
5. Chang H, Fitzpatrick JM. A technique for accurate magnetic resonance imaging in the presence of field inhomogeneities. *IEEE Transactions on Medical Imaging*. 1992;11(3):319–329.
6. Andersson J, Skare S, Ashburner J. How to correct susceptibility distortions in spin-echo echo-planar images: application to diffusion tensor imaging. *NeuroImage*. 2003;20(2):870–888.
7. Holland D, Kuperman JM, Dale AM. Efficient correction of inhomogeneous static magnetic field-induced distortion in Echo Planar Imaging. *NeuroImage*. 2010;50(1):175–183.
8. Modersitzki J. FAIR: Flexible Algorithms for Image Registration. Society for Industrial and Applied Mathematics (SIAM); 2009.
9. Mohammadi S, Nagy Z, Hutton C, Josephs O, Weiskopf N. Correction of vibration artifacts in DTI using phase-encoding reversal (COVIPER). *Magnetic Resonance in Medicine*. 2012;68(3):882–889.
10. Jezzard P, Barnett A, Pierpaoli C. Characterization of and correction for eddy current artifacts in echo planar diffusion imaging. *Magnetic resonance in medicine*. 2005;39(5):801–812.